Journal of Power Sources 234 (2013) 208–216

Contents lists available at SciVerse ScienceDirect

Journal of Power Sources

journal homepage: www.elsevier.com/locate/jpowsour

Electrochemical characterization and equivalent circuit modeling of single-walled carbon nanotube (SWCNT) coated electrodes

Jinhee Kang [a], John Wen [a,*], Shesha H. Jayaram [b], Xiaohui Wang [c], Shih-Ken Chen [d]

[a] Mechanical & Mechatronics Engineering, University of Waterloo, 200 University Avenue West, Waterloo, ON N2L 3G1, Canada
[b] Electrical and Computer Engineering, University of Waterloo, 200 University Avenue West, Waterloo, ON N2L 3G1, Canada
[c] Canadian Regional Engineering Centre, GM of Canada Ltd., General Motors Company, 1908 Colonel Sam Drive, Oshawa, ON L1H 8P7, Canada
[d] General Motors R&D Center, MC 480-106-390, 30500 Mound Road, Warren, MI 48090, USA

HIGHLIGHTS

- Single-walled carbon nanotube electrodes.
- Electro-chemical characterizations.
- Equivalent circuit modeling.

ARTICLE INFO

Article history:
Received 31 August 2012
Received in revised form
9 January 2013
Accepted 11 January 2013
Available online 17 January 2013

Keywords:
Single walled carbon nanotubes
Electrode
Pore distribution
Cyclic voltammetry
Circuit model
Impedance spectroscopy

ABSTRACT

Single-walled carbon nanotube (SWCNT) coated electrodes are fabricated from functionalized suspensions with different pH values. Their electrochemical properties are characterized using cyclic voltammetry and electrochemical impedance spectroscopy. The effects of the pH value of the suspension on electrochemical performances are investigated through examining the microstructures of the SWCNT films and their BET specific areas and pore volume and size distributions. Both these specific areas and pore size distributions are found being important in determining the specific capacitances of SWCNT coated electrodes. An equivalent circuit model is developed for these electrodes using the measured electrochemical impedance data. It is found that the functionalized nanotube suspensions with higher pH values produce more desirable nanostructured electrodes with the increased specific capacitance and reduced electrode resistance. The role of the pseudo-capacitance which arises from the functionalization group is also discussed.

1. Introduction

The manufacturing technologies of nanostructured electrodes for energy conversion and storage devices have been recently developed through utilizing a variety of carbon materials [1–5]. Owing to its advantages of low material and manufacturing costs, high surface area and low resistivity, the activated carbon is one of the most popular electrode materials found in commercial devices which possess satisfying electrical, chemical and thermal properties and relatively high capacitances. Typically as demonstrated in Fig. 1, a porous carbon electrode is fabricated on a metallic current collector and reaches into an electrolyte which can be aqueous or organic. The porous electrode is an important component for providing the charge storage sites and ion transport channels along the interface between the solid electrode surface and the liquid electrolyte. In the concept of electrochemical double layer capacitor (EDLC) model, firstly defined by Helmholtz [6], the charge is stored on the surface of electrodes. This model is later detailed by Guoy [7] and Stern [8] who introduced the diffusion layer to evaluate the influence of ions in electrolytes, in addition to the Helmholtz layer. Based on those models, the porous electrode plays a dominant role in determining the specific capacitance of the electrical component [9]. The literature has also found that the activated carbon can exhibit large specific surface areas ranging from 1000 to 3000 $m^2 g^{-1}$, while a limited accessibility of charges to these surface areas may exist [10]. It hence becomes straightforward that, as shown in Fig. 1, ions need to, through their transportation in the porous carbon structure, access to the storage carbon surface

* Corresponding author. Tel.: +1 519 888 4567x38362; fax: +1 519 885 5862.
E-mail address: john.wen@uwaterloo.ca (J. Wen).

0378-7753/$ – see front matter © 2013 Elsevier B.V. All rights reserved.
http://dx.doi.org/10.1016/j.jpowsour.2013.01.058

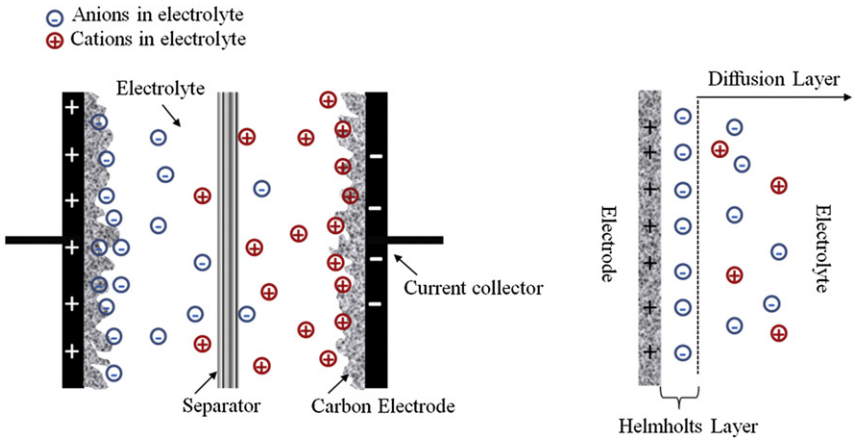

Fig. 1. Schematics of an electrochemical double layer supercapacitor and the electrode/electrolyte interface model.

effectively and eventually these ions are electro-chemically adsorbed on that surface. The structural properties of the pores of the activated carbon, therefore, are among critical parameters to determine energy and power densities of the supercapacitor utilizing the activated carbon electrodes. It has been shown that the commercially available activated carbon products, having high surface areas, unfortunately possess a poorer accessible porosity for electrolyte ions and can result in lower capacitances [11,12]. The control of these pore sizes is therefore extremely important for optimizing the ion's transport channel and subsequently to increase the ion storage capacity on the nanostructured electrodes.

In order to fabricate high-performance electrodes with more assessable pores, a variety of carbon nanostructures including single walled (SWCNTs) and multi-walled carbon nanotubes (MWCNTs) and graphenes have recently drawn much attention [13–17]. In comparison with activated carbons, carbon nanotubes (CNTs) have a moderate specific surface area (400–800 $m^2\ g^{-1}$), which is about half of the value of activated carbons and a controllable porosity when patterned into electrodes. A high capacitance (about 180 $F\ g^{-1}$) was reported for CNT based electrodes [14] and much research effort has been committed to produce CNT based electrodes with uniformly distributed and better accessible pore structures [17–21]. It has become really essential to develop an appropriate processing technology which is able to coat CNTs with right structural geometries (e.g., large surface area, uniform pores with optimized ion accessible paths) and suitable for mass production. One of promising fabrication techniques for producing CNT coated electrodes is the electrophoretic deposition (EPD) method, which is principally a combination of electrophoresis and deposition processes [22–29]. In the first step, charged individual tubes suspending in a liquid are forced to move toward an oppositely charged electrode under an external electric field. In the second step, the nanotubes are deposited and collected at the electrode surface and form a thin film. The attraction of this method lies in its simplicity and feasibility for manufacturing homogenous composite coatings on complex shapes of substrates. In addition, EPD has shown its advantages of the fast processing rate, simple apparatus and suitability for large-scale production [23].

In literature detailed investigations have been carried out to study the correlations between electrochemical properties of the deposited CNT films and the EPD processing parameters such as the temperature and period. The previous studies [24,26] revealed that the EPD deposition rate is dependent on the electrophoretic mobility, μ ($m^2\ V^{-1}\ s^{-1}$), the field strength, E (Vm), the processing temperature (°C) and the processing period (min), while the electrophoretic mobility is determined by the properties of suspending particles such as their surface charges (indicated by the zeta potential, ζ (V)) as well as the properties of suspensions including the viscosity of the liquid. In other words, successful EPD processing requires a well dispersed colloidal suspension. For CNTs, the acid-treatment has been often applied through mixing a certain oxidizing agent (e.g., HNO_3/H_2SO_4, O_3, $KMnO_4$ or H_2O_2) with CNT suspensions [30–32]. The presence of hydrophilic oxygen-containing functional groups on the surface of acid oxidized CNTs generates either negative or positive surface charges and helps disperse individual CNTs in the suspension. Under an external electrical field, these charged CNTs are driven toward and deposited on the anode or cathode. It was found that the extent of surface charges measured in the term of Zeta potential correlates to pronounced differences in the aquatic stability, mobility, and aggregation states of suspending CNTs [33–35]. Moreover, the surface charges of CNTs vary with the levels of oxidation (indicated by the surface oxygen concentration on CNTs in the form of COOH, C–OH or C=O) and pH values in the suspension. It was shown in literature [32,33] that, the nanotubes are negatively charged if the pH value is greater than 3, and more negative charges will be homogenously accumulated on the surface of CNTs if the pH value becomes larger [35]. In summary, by varying the pH value of the suspension, the surface charge state of acid-treated CNTs can be changed and subsequently the transport properties of CNTs and the deposition rate of EPD will be altered.

The main objective of this study was to characterize the electrochemical properties of EPD processed CNT coatings from suspensions with different pH values. It was expected that the electrolyte accessibility in CNT coatings changes with the surface morphology and porous structures. The as-produced electrodes from various pH values would therefore exhibit distinguishable electrochemical properties. The second objective was to develop an equivalent circuit model for such SWCNT coated electrodes through measuring the cyclic voltammetry and electrochemical impedances of different coatings. This model is useful for later studies on characterizing of electrochemical properties of supercapacitors and recognizing complex electrochemical reactions in SWCNT electrodes [36].

2. Experimental

The SWCNT powder used in this work was supplied by Nano-C Inc. with a purity of 97%. The as-received samples were first acid functionalized using a mixture of nitric (HNO_3) and sulfuric (H_2SO_4) acids with a ratio of 3:1 (Sigma–Aldrich). 10 mL of this mixture was then added to 250 mg of the SWCNT powder and kept for 30 min to complete the carboxyl functionalization process [37]. During this

process the –COOH functional groups were added to the defect and end sites of SWCNTs. After the functionalization the mixture was diluted with de-ionized water and washed through a filter to remove the residual acidic solution from SWCNTs. Then more de-ionized water was added and an aqueous suspension was produced with a concentration of approximately 0.5 mg SWCNTs/ml H_2O. The pH value of the derived SWCNT suspension was adjusted by adding 1 M sodium hydroxide (NaOH) solution at room temperature (22 °C). These suspensions were then placed in a Branson 5210 Ultrasonic cleaner for 6 h. Finally the suspensions were centrifuged at 4000 rpm for 15 min to remove undesirable particles and agglomerated SWCNT bundles. In each step of the filtration, centrifugation and decantation, the pH value was closely monitored using a PHH-830 meter and re-adjusted if necessary. Finally, three suspensions with the pH values of 4, 7 and 10, respectively, were prepared and used in the EPD processing.

The details on EPD processing of SWCNT suspensions can be found in the literature [22,28] therefore only a brief description is provided here. The SWCNT coated electrodes were fabricated with a working distance of 1 cm between two current collectors made of stainless steel (70% Fe, 19% Cr, and 11% Ni: wt %, Alfa Aesar). EPD was carried out under a range of processing conditions including a deposition time between 3 and 30 min, room temperatures and three pH values. A DC power supply of 40 V was used. All electrodes were made with a coated area of 10 mm × 10 mm × 0.1 mm. The electrodes were finally dried on the hot plate for 30 min at 90 °C to remove moisture and solidify the SWCNT network.

In order to determine the surface area and the pore size distribution of the SWCNT network, nitrogen adsorption measurements were performed at 77 K using a Micromeritics Flowsorb surface area analyser. This analyser quantifies the Brunauer–Emmett–Teller (BET-N_2) surface area and Barrett–Joyner–Halenda (BJH) pore size distributions. More specifically, the specific surface area (S_{BET}) was derived from the BET theory [38] when the relative pressure (p/p_0) of nitrogen was set up to 0.3. The pore size distribution was determined by the same adsorption procedure from the gas adsorption isotherms. It has been well received that from the literature, for samples possessing a pore size range of 2 nm–50 nm, the BJH method is quite accurate. This method employs the Kelvin equation for describing the relationship between the individual pressure value and specified pore size when a gaseous adsorbent spontaneously condenses in a pore. By monitoring the incrementally increasing pressure, the pore size distribution can be derived and so does the pore volume distribution. The total volume of pores (V_{tot}) was obtained by summing up the adsorption pore volume up to the saturation pressure $p/p_0 = 0.99$. The pore surface area was then calculated by the measured BJH pore size. Detailed descriptions on how to determine the incremental pore volume and surface area against each average pore diameter from the adsorption isotherms can be found from literature [39]. In our study this task was performed using the software provided with the analyzer. The surface morphology of the EPD processed SWCNT film was characterized by a field emission scanning electron microscope (LEO 1530 FE-SEM) for visualizing the micro-porosity. The electrochemical properties of these electrodes were evaluated using the cyclic voltammetry (CV) measured by a Gamry Reference 3000 Potentiostat within a potential range of −0.2 to 0.8 V at the scan rate of 20 mV s^{-1}. Electrochemical impedance spectroscopy (EIS) was performed on the same potentiostat using the EIS 300 software. The frequency range was set from 0.1 Hz to 100 kHz. Fig. 2 shows the schematic of a three-electrode cell where the CV curves and EIS data were measured. The cell includes the working (SWCNT coated), counter (platinum) and reference (Ag/AgCl) electrodes. An aqueous 1 M H_2SO_4 solution was used as the electrolyte in the cell at room temperature.

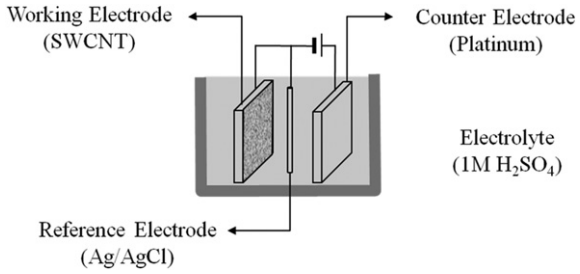

Fig. 2. Schematic diagram of the three-electrodes test cell.

3. Results and discussion

3.1. SWCNT suspensions with different pH values

The effect of different pH values on the SWCNT suspension is visible and shown in Fig. 3. As mentioned earlier, all three suspensions were prepared from the same sample with the concentration of 0.5 mg SWCNTs per 1 mL of water. Then an extra amount of NaOH or HCl was added in order to reach different pH values in the suspension. It was expected that the higher pH value produced more negatively charged SWCNTs in the suspension, and consequently SWCNTs are dispersed homogenously in higher pH conditions. Finally these samples were processed using the ultrasonic cleaner and larger agglomerates were filtered out. This sample preparation procedure resulted in different appearances and concentrations of SWCNTs in three suspensions. In general, the suspension with a lower pH value (such as pH = 4) contains less charged individual tubes and more nanotube agglomerates, and the total quantity of CNTs in this suspension is small. In contrast, the suspension with a higher pH value (e.g., pH = 10) contains less agglomerates and more individual nanotubes owing to higher surface charges (Zeta potential). The observation in Fig. 3, in agreement with the previous studies [34,35], reveals the higher pH values facilitate the better dispersion of SWCNTs, which can be attributed to an easier ionization of the carboxylic (COOH) group in these suspensions with large pH values. The more carboxylate ($-COO^-$) groups were obtained on the surface, the heavier charging of individual tubes was achieved, which led to the more effective dispersion of SWCNTs. Consequently after filtering, the higher pH suspension has the greater concentration of dispersed SWCNTs in it. In addition, the previous studies [33,37] suggested that, the electrophoretic mobility and surface charges of acid-treated CNTs increase with the increasing pH value. These

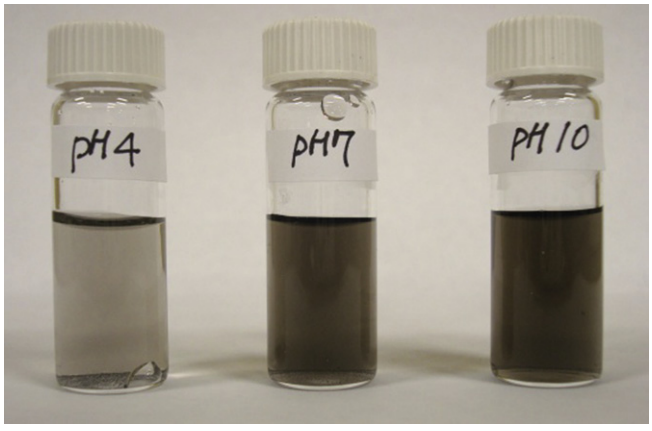

Fig. 3. Photographs of SWCNT suspensions at pH 4, 7 and 10, respectively.

parameters, together with the quantity of available SWCNTs in the suspension, undoubtedly affect the deposition rate of the EPD process.

3.2. Influence of pH values of the suspensions to EPD rates

Using the suspensions with different pH values, SWCNT coated electrodes were fabricated by the EPD process at room temperature and with controlled processing times. The optical images of these as-produced electrodes showed that for the same processing time, the electrodes processed at higher pH values are much darker than other electrodes at lower pH values, and they also have a greater coverage and a better uniformity. The microstructures of these electrodes were further examined using FE-SEM. Fig. 4 shows the FE-SEM images of SWCNT networks obtained from suspensions with different pH values and for two processing times, 3 min and 30 min, respectively. The inserted figure shows a high-resolution SEM image of individual tubes obtained from a shorter processing time (30 s). In general, increasing the processing time produces thicker SWCNT films on the substrate and deposit more material as the electrode [40,41]. For the processing time of 3 min as described in Fig. 4(a), the pH 4 suspension produced less material on the substrate while more individual SWCNTs were deposited in the pH 10 suspension. In addition, for this short processing time of 3 min, the difference in surface morphology from various pH suspensions was insignificant due to a limit amount of nanotubes deposited on the substrate. The SEM images, from Fig. 4(a) for pH 4 and pH 10, however, still show the distinguishable appearance of these microstructures formed from EPD. On the pH 4 image, there are obviously many flakelet structures which were formed from the deposition of nanotube bundles, due to in-sufficient dispersion of individual nanotubes under low pH conditions. On the pH 10 image, however, the nanotubes and bundles are clearly observed directly on the electrode, which confirms a better deposition resulted from a satisfying dispersion of individual tubes with a higher pH value. For the processing time of 30 min (Fig. 4(b)), micro-structures of CNT bundles appeared on all three samples but the pH 10 suspension produced more individual tubes and a smoother surface morphology. Fig. 4(c) explains the deposition mechanism of SWCNTs in these suspensions with different pH values. First, in agreement with the previous observation [40], these films produced from shorter EPD processing times possess much less amounts of SWCNTs than ones produced with long EPD times. Secondly, for the pH 4 suspension, more agglomerates exist and the deposition happens by carrying with larger SWCNT bundles, which causes the formation of irregular microstructures on the substrate. Moreover, the less material available in the suspension results in a slower deposition rate and brings about less deposited material. For the pH 10 suspension, more individual tubes exist in the suspension and their surface charging levels are higher. This situation results in a larger deposition rate and a well ordered deposition film is produced. For the pH 7 suspension, the situation becomes a bit complicated due to the availability of bigger agglomerates in the suspension and the faster deposition rate of such structures. More micro-structures were observed on the coating and the morphology became less organized. The similar finding was reported in EPD processing of SiO_2 films [42]. Well dispersed particles were found in the higher pH value suspensions and more uniform films with the low surface roughness were produced. In contrast, unstable suspensions with low pH values could not produce thick films due to

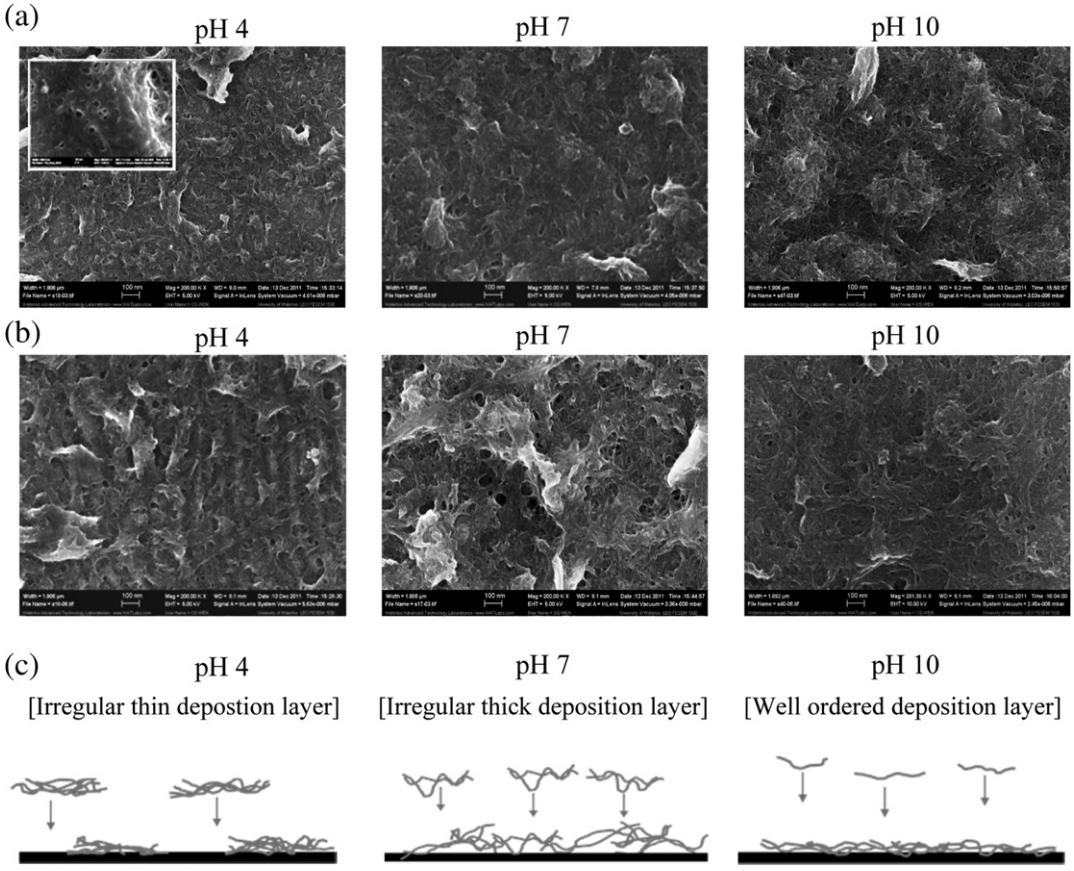

Fig. 4. FE-SEM images of SWCNT electrodes processed from suspensions with different pH values and with the EPD period of (a) 3 min, (b) 30 min, respectively. (c) The qualitative illustration of the deposition mechanisms with varying pH values.

sedimentation. With a moderate pH value particle agglomerates in EPD processing exhibited a high surface roughness.

It is important to quantify the effects of the pH value on the EPD deposition rate. In literature [24], the kinetics of EPD processing was described by Hamaker's law given by

$$\omega = \int_{t2}^{t1} f\mu EAC\mathrm{d}t \tag{1}$$

where the deposition rate (ω) is expressed as a function of the concentration of charged particles in the suspension (C), the electrical field strength (E), the electrophoretic mobility (μ), the area for deposition (A) and a constant f. The electrophoretic mobility, which depends on both these properties of particles and the liquid, can be calculated by

$$\mu = \frac{\varepsilon\varepsilon_0\zeta}{\eta} \tag{2}$$

where ε is the dielectric constant of the liquid, ε_0 is the vacuum permittivity, ζ is the zeta potential that is proportional to the surface charge of the particles [43], and η is the viscosity of the liquid. Equation (2) shows the strong dependence of the electrophoretic mobility on the zeta potential of suspending SWCNTs. The suspension with a higher pH value contains CNTs with more surface charges and results in the higher zeta potential and hence exhibits a better electrophoretic mobility. In addition, the concentration of charged nanotubes is higher in this suspension. Both factors, according to Equation (1), will accelerate the EPD deposition rate in suspensions with high pH values.

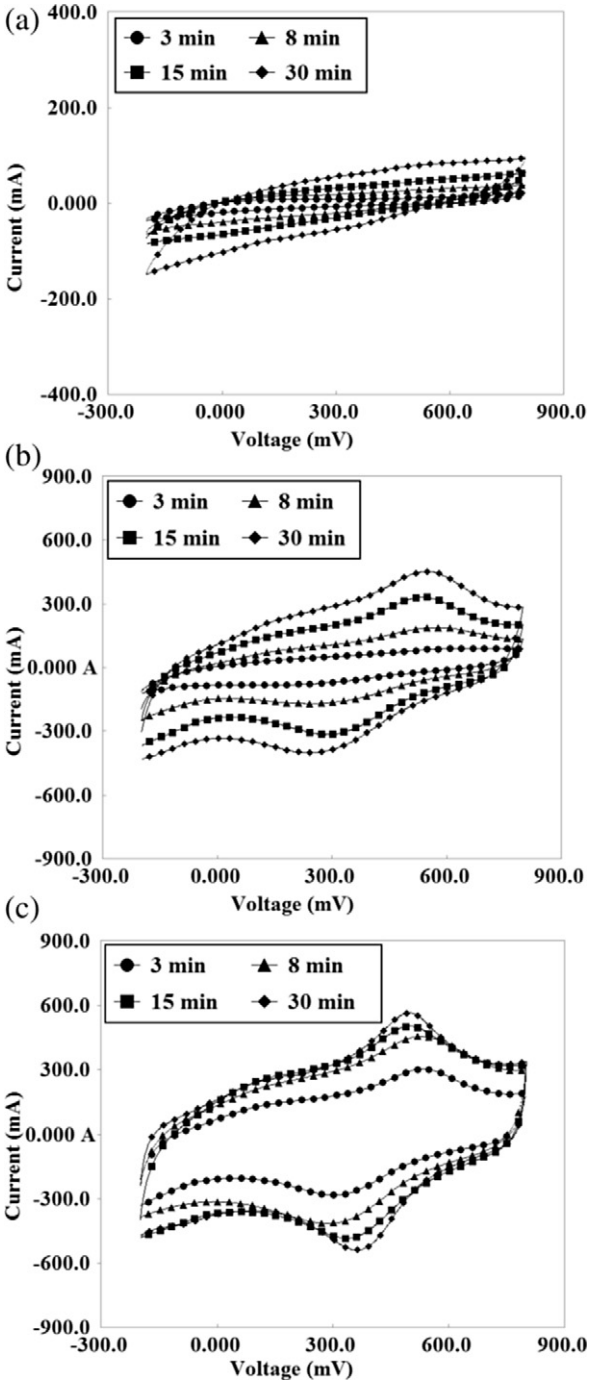

Fig. 5. Cyclic voltammograms of SWCNT electrodes, in 1 M H_2SO_4 with various pH values, (a) pH 4, (b) pH 7 and (c) pH 10.

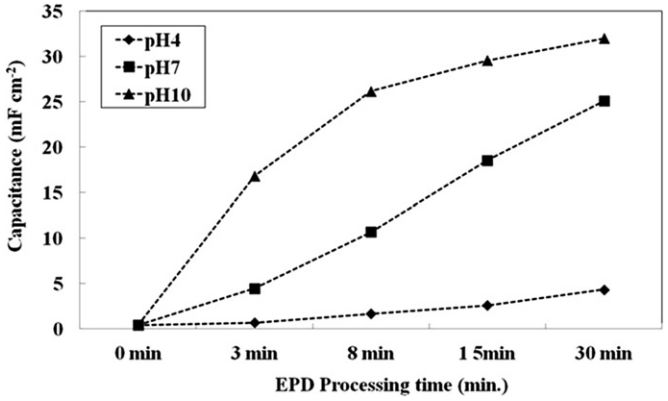

Fig. 6. The dependence of the capacitance (evaluated by cyclic voltammetry) on the EPD processing times for varying pH values.

3.3. Electrochemical characterization of SWCNT electrodes

Cyclic voltammetry (CV) graphs of these SWCNT coated electrodes derived from different pH suspensions are shown in Fig. 5. Note that the scale of the y axis in Fig. 5(a) is close to half of that of Fig. 5(b). These figures show that the bumped regions are less significant for electrodes produced from lower pH values, due to less surface charging (and less carboxylate groups) of the SWCNTs. Up to 30 min, the pH 10 suspension produced the largest area enclosed by the CV curves. For the pH 7 and pH 10 cases, the bumped regions, which are attributed to the pseudo-faradaic reactions caused by the carboxylate groups [44,45], have been larger corresponding to the following reactions:

$$-\mathrm{COOH} \Leftrightarrow -\mathrm{COO} + \mathrm{H}^+ + \mathrm{e}^- \tag{3}$$

$$>\mathrm{C{=}O} + \mathrm{e}^- \Leftrightarrow \ >\mathrm{C{-}O}^- \tag{4}$$

From the CV graphs reported in Fig. 5 the specific capacitances were calculated in regard to the geometric area (1 cm^2) of the

Table 1
BET surface areas, total pore volumes and average pore diameters of SWCNT electrodes processed with different pH conditions.

Sample (pH)	BET surface area, S_{BET} ($m^2\ g^{-1}$)	Total pore volume, V_{tot} ($cm^3\ g^{-1}$)	Average pore diameter (nm)
pH 4	601	0.32	4.2
pH 7	642	0.425	3.9
pH 10	820	0.629	2.7

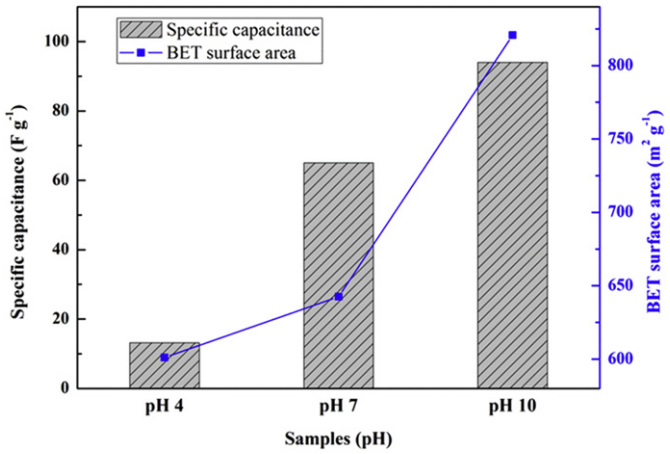

Fig. 7. Specific capacitance (F g^{-1}) and BET surface area of SWCNT electrodes fabricated with different pH values.

electrode. The results are shown in Fig. 6. The SWCNT coated electrodes derived from the pH 10 suspension exhibit the highest capacitance (mF cm^{-2}) for all processing times ranging from 0 to 30 min. The value of specific capacitance increases much faster for the pH 10 suspension, compared to two other suspensions. The pH 4 curves show the lowest specific capacitances with less pseudo-faradaic effects in Fig. 5(a). The behaviors of different electrodes were expected from the distinct EPD rates and the different amounts of deposited material on the electrodes from various suspensions.

3.4. Specific capacitance, BET surface area and pore volume

As mentioned earlier, there is a strong correlation between the specific surface areas of carbon nanostructures and their specific capacitances. The BET measurements were carried out in order to assess this relationship. All measurements were done for different pH samples with the same EPD processing time of 30 min. Table 1 summaries the BET specific surface areas (S_{BET}), total pore volume (V_{tot}) and average pore diameters obtained for three pH suspensions. With increasing the pH value, the specific surface area of SWCNT network increases; whereas, the average pore diameter decreases. The electrode derived from the pH 10 suspension shows the highest BET surface area (820 m^2 g^{-1}) and the smallest pore size (2.7 nm). Fig. 7 plots the increasing trends of the specific capacitance and the surface areas for three pH cases, and these two parameters do not show a linear interdependence. This implies the essential role of pore accessibilities in ion transportation and storage [12].

In order to investigate the contribution of the pore accessibility to specific capacitance, the pore volumes and pore areas of SWCNT networks on three electrodes were measured from nitrogen adsorption using the BJH method. The data are plot in Fig. 8 against the average pore diameter. As shown, the pore surface area is greater for the electrodes fabricated from the larger pH values. For the pore volume, there are distinctly two regions which can be observed in Fig. 8(b). For smaller pores with their diameters less than 4 nm, the pH 10 electrode has the largest number of such pores, while for larger pores with their diameters greater than 4 nm, the pH 4 electrode has the largest pore number. In comparison with Fig. 7 which shows the pH 10 electrode has the largest specific capacitance, it can be concluded that the availability of larger pores in the wide size range (5–50 nm) do not significantly affect the specific capacitance, while the accessibility to smaller pores, corresponding to the average pore diameter below 4 nm, is dominant in determining the specific capacitance. This complicate dependence of the accessibility to small pores on the pH value of the EPD suspensions result in a non-linear relationship between the specific capacitance and the specific surface area, as shown in Fig. 7. It has been well received that, from the literature, the surface area is not the sole parameter determining the specific capacitance for carbon nanostructure based electrodes. The other critical parameter is pore distribution. Therefore, a nonlinear relationship was expected. Fig. 7 intends to show this relationship by plotting the increasing trend of the specific capacitance and the BET surface area from these three pH samples. These trends shown in Fig. 7 suggest, the specific capacitance of SWCNT based electrodes is determined by both the specific surface area and their pore size distribution. Note that the pore accessibility depends not only on the pore distribution on the electrode but also on the type of electrolytes. In this study, the optimum pore sizes for these EPD processed SWCNT electrodes are between 2 and 4 nm and lead to the highest ion accessibility. More investigations are expected for characterizing the optimum pore size for other types of electrolytes such as organic or non-aqueous ones.

3.5. Electrochemical impedance resistance and equivalent circuit model

In addition to CV graphs, the EIS measurement is important for characterizing the impedance resistance of SWCNT coated electrodes. A typical Nyquist plot in the EIS analysis for an electrochemical double-layer capacitor (EDLC) is shown in Fig. 9(a). This curve consists of a semicircle at the high frequencies followed by a 45° inclination at the modest frequencies and with a vertical line at low frequencies. For a porous or rough electrode surface, an arc can replace the semicircle, which is attributed to the rise of the constant phase element (CPE) in the high frequency region. In the low frequency region, the semi-infinite diffusion of ions can become significant for determining the diffusion impedance of a porous electrode. This impedance, created by ion diffusion in

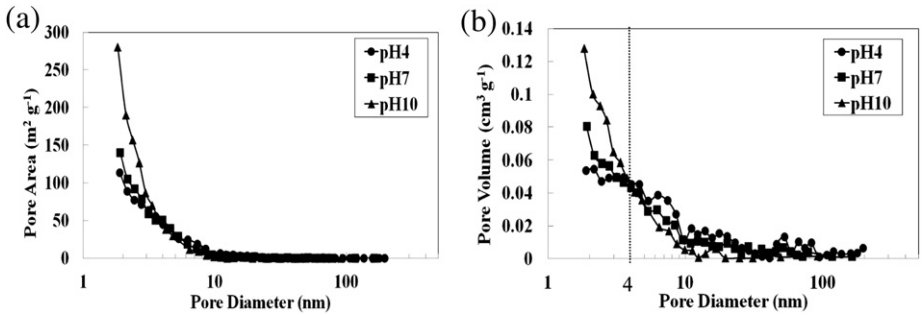

Fig. 8. Measured BJH pore size distributions of SWCNT electrodes fabricated with different pH values: (a) pore area and (b) pore volume.

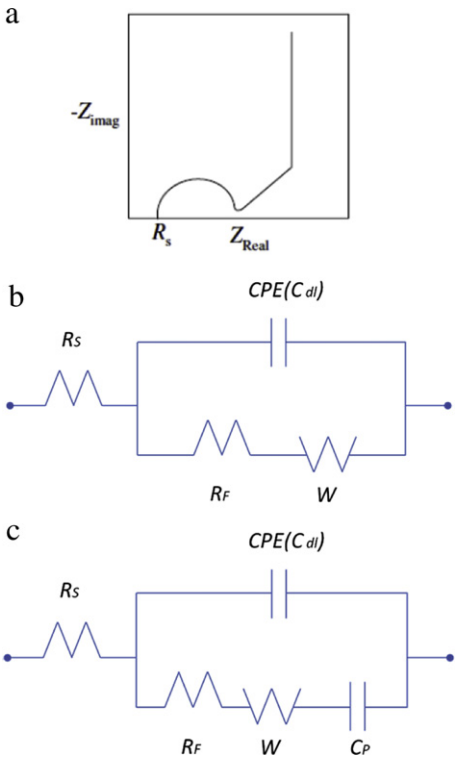

Fig. 9. (a) Experimental Nyquist plot of typical EDLCs. (b) The typical equivalent circuit model for EDLCs. (c) The practical equivalent circuit model for EDLCs including a pseudo-capacitance (C_P).

a porous structure, is known as Warburg impedance and usually appears as a straight line with a slope of 45°. The Warburg impedance will not appear when the diffusion of ions into the pores is negligible at the high frequency region. On the other hand, a strong ion diffuses into the porous network will make the Nyquist plot a vertical line. The above EIS characteristics can be represented by a few electrical components when an equivalent circuit model is needed to describe the impedance behavior of an electrode. Such a circuit model is shown in Fig. 9(b) for the EDLC where a capacitor (CPE) is parallel with a Warburg impedance (W), associated with a Faradic resistance (R_F) to account for the accessibility of ions within the porous structures and surface functionalities or polarization resistance. A series resistance R_S is introduced to consider the resistance of the electrolyte and the contact resistance at the interface between porous electrodes and the current collector. If the role of pseudo-capacitance (C_P) cannot be neglected and the contributions of reduction and oxidation (redox) reactions of surface functional groups occurring at the surface of the electrode should be considered [30,44], Fig. 9(c) is often used for developing an equivalent circuit model of some practical electrodes.

Using the EIS 300 software (Gamry Ins.), the Nyquist plots were made for the SWCNT coated electrodes fabricated from these suspensions with three pH values. 1 M H_2SO_4 was used as the electrolyte and the measurements were performed for two EPD processing times of 3 min and 30 min, respectively. Fig. 10(a) and (b) shows the Nyquist plots of 3 min electrodes in the entire range of tested frequencies ranging from 0.1 Hz to 100 kHz. The zoomed figure emphasizes the high frequency zone. On these plots, the diameter of semicircle is referred as R_F while the high frequency intercept on the Z_{real} axis represents the sum of R_S. The pH 4

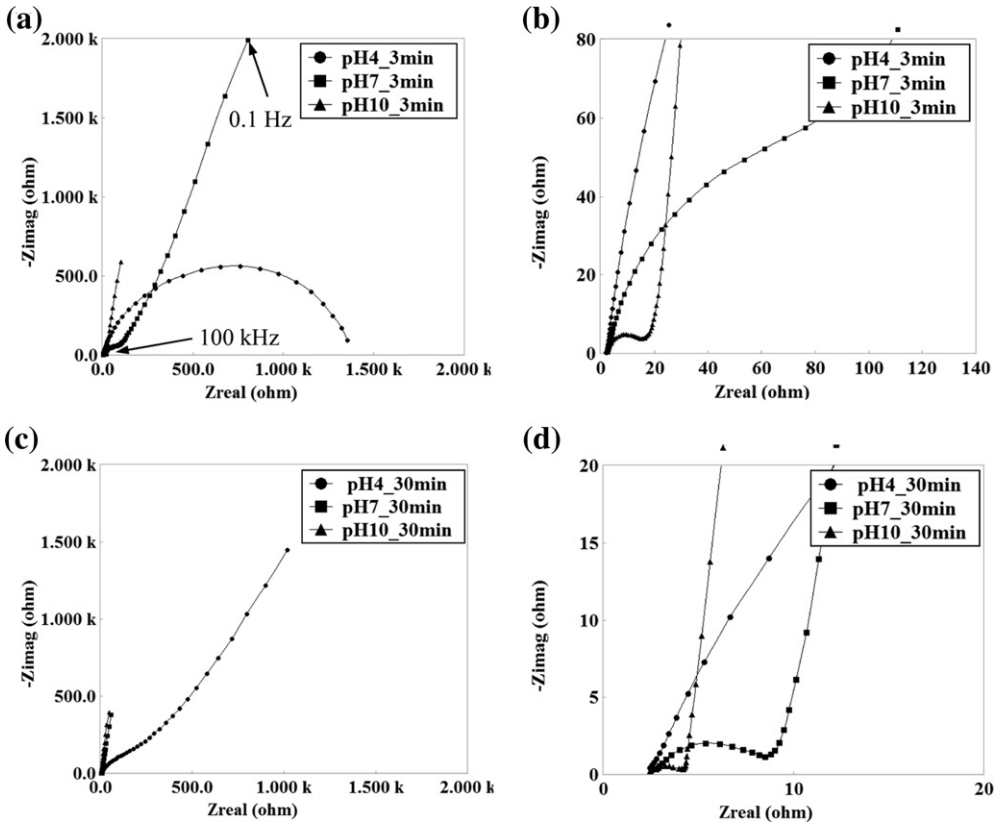

Fig. 10. (a) Nyquist plots for the SWCNT electrodes with different pH values at the EPD processing time of 3 min. (b) Enlarged sections of the Nyquist plots at high frequency for (a). (c) Nyquist plots for the SWCNT electrodes with different pH values at the EPD processing time of 30 min. (d) Enlarged sections of the Nyquist plots at high frequency for (c).

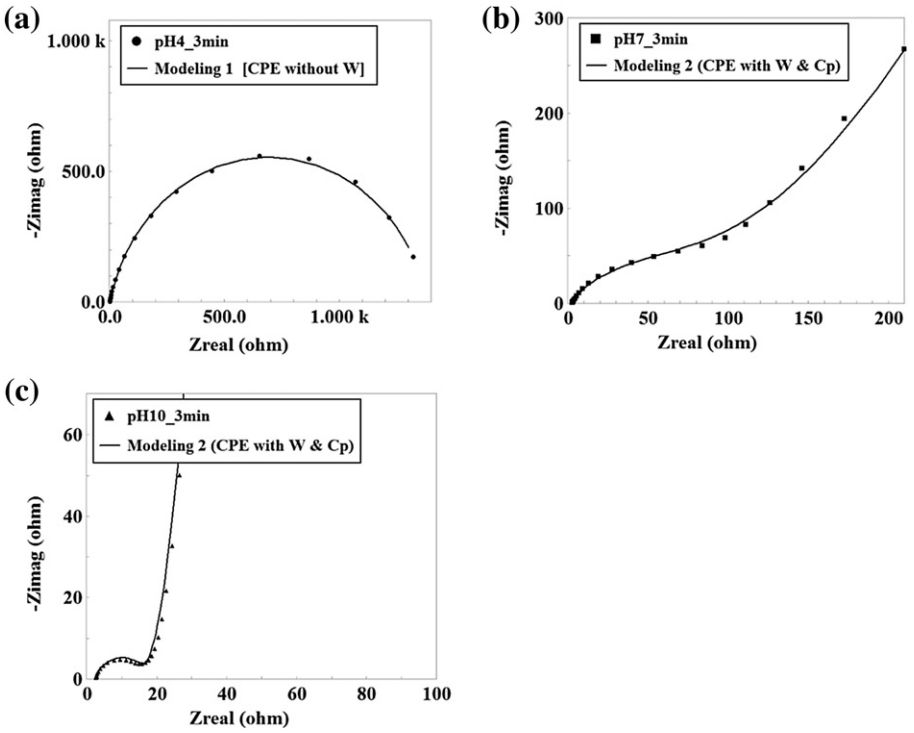

Fig. 11. Correlation between Nyquist plots with different pH values: (a) pH 4, (b) pH 7 and (c) pH 10.

electrode shows an almost complete semicircle which reveals a less porous electrode after the short EPD processing time of 3 min. On the other hand, both pH 7 and pH 10 electrodes show a part of arc followed by a straight line showing a sharp increase in the imaginary part of the impedance at lower frequencies, which are representative of ion diffusion dominant processes. Especially the pH 10 electrode shows its linear EIS performance over a wider range of frequencies. It is also noticed that the relatively large values of R_F exist for the lower pH value electrodes. This is attributed to the poorer accessibility of ions to the pores on the electrodes fabricated from lower pH suspensions. Fig. 10(c) and (d) shows the Nyquist plots of 30 min electrodes. In comparison with the similar observations in Fig. 10(a) and (b), both the pH 7 and pH 10 electrodes show very large capacitances at high frequencies.

Using the measured EIS data and adapting the equivalent circuit model shown in Fig. 9, the values of C_P, R_S and R_F were fitted into the Nyquist curves. Also, the impedance of a CPE can be represented as defined below:

$$Z = (1/Y_0)/(j\omega)^{\alpha} \quad 0 < \alpha < 1 \tag{5}$$

For a double layer capacitor, the constant Y_0 indicates the capacitance and the exponent α is less than 1. Fig. 11 shows the comparisons among the Nyquist plots of electrodes which were fabricated from different pH values. Table 2 shows the proposed equivalent circuit models. Table 3 summaries the values of three parameters determined from different electrodes. Note that the C_P values of the pH 4 electrodes are extremely small due to very limited amount of surface charges on the electrode (and less

Table 2
Proposed equivalent circuits models for SWCNT electrodes fabricated from different pH values.

Equivalent circuit model for SWCNT electrodes	
Model 1	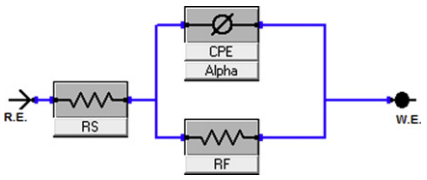
Model 2	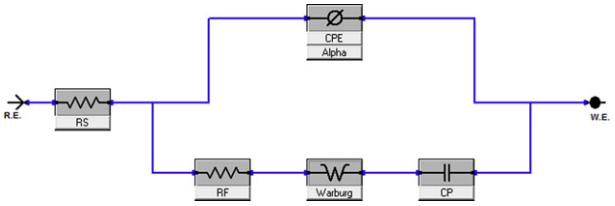

Table 3
Equivalent circuit parameters (C_P, R_S & R_F) obtained from the modeling results.

	3 min				30 min		
	C_P	R_S	R_F	α	C_P	R_S	R_F
pH 4	–	2.1	1351.3	0.861	$1.6e^{-7}$	2.2	177.3
pH 7	$9.6e^{-4}$	2.4	74.6	0.81	$3.4e^{-3}$	2.4	5.5
pH 10	$2.9e^{-3}$	2.4	11.8	0.794	$4.6e^{-3}$	2.5	1.5

pseudo-faradaic effect). The pH 10 electrodes with 30 min processing time show the largest C_P, which shows the existence of the pseudo-capacitance. It can be seen that R_F decreases as increasing the pH value of the suspensions, while R_S slightly increases. This can be explained using the pore distributions shown in Fig. 8. The SWCNT coated electrode from the high pH value exhibits a lower R_F because it possesses a better electrolyte's accessibility to pores in the range of 2–4 nm. The contact resistance R_S at the interface may increase due to more micro-structures formed on the electrode. These observations suggest that, as the pH value increases, the sharp increase of the imaginary part of the impedance resistance appears at lower frequencies and extends to the entire frequency range. In addition, the SWCNT networks fabricated from higher pH suspensions show their larger specific capacitances which are attributed to more effective pore volumes. Moreover, pseudo-capacitances (C_P) were found important on these electrodes fabricated from higher pH suspensions. As increased pH value, the surface functionalization group contributes more pseudo-capacitance.

4. Conclusion

SWCNT coated electrodes were fabricated from functionalized CNT suspensions with various pH values using the electrophoretic deposition method (EPD). EPD processing at higher pH values yielded SWCNT electrodes with increased surface areas and more effective pore volumes, while both contributed to the increase in the specific capacitances of these electrodes. The measurements of electrochemical impedance resistance revealed the rapid increase of the imaginary part of the impedance resistance when the electrode was fabricated with higher pH values. The finding from the equivalent circuit model further confirmed that the higher pH treatment is desired not only to reduce the SWCNT electrode resistance (R_F) but also to introduce a complementary effect of pseudo-capacitance. In addition, the optimized pore size distribution through modifying pH values could enhance the performance of SWCNT electrodes. Moreover, the decrease of the internal resistance was achieved when desirable nanostructured electrodes were fabricated from the EPD process. This investigation of impedances of the SWCNT electrodes fabricated from functionalized suspensions with different pH values will help optimize their electrochemical properties for designing high energy density devices.

Acknowledgments

The authors would like to acknowledge the financial support of Ontario Research Fund (ORF), Automotive Partnership Canada (APC), Natural Sciences and Engineering Research Council of Canada (NSERC) and General Motors (GM).

References

[1] H. Chen, T.N. Cong, W. Yang, Y. Ding, Progress in Natural Science 19 (2009) 291–312.
[2] F.-Y. Kang, Y.-B. He, B.-H. Li, H.-D. Du, New Carbon Materials 26 (2011) 246–254.
[3] Y. Zhai, Y. Dou, D. Zhao, S. Dai, Advanced Materials 23 (2011) 4828–4850.
[4] A.G. Pandolfo, A.F. Hollenkamp, Journal of Power Sources 157 (2006) 11–27.
[5] M. Inagaki, H. Konno, O. Tanaike, Journal of Power Sources 195 (2010) 7880–7903.
[6] H.V. Helmholtz, Annalen der Physik 165 (1853) 211–233.
[7] G. Gouy, Journal of Physics 9 (1910) 441–467.
[8] O. Stern, Zeitschrift Fur Elektrochemie Und Angewandte Physikalische Chemie 30 (1924) 508–516.
[9] Conway, Electrochemical Supercapacitors: Scientific Fundamentals and Technological Applications, Kluwer Academic/Plenum Press, New York, 1999.
[10] E. Frackowiak, Physical Chemistry Chemical Physics 9 (2007) 1774–1785.
[11] D. Qu, H. Shi, Journal of Power Sources 74 (1998) 99–107.
[12] J. Gamby, P.L. Taberna, P. Simon, J.F. Fauvarque, M. Chesneau, Journal of Power Sources 101 (2001) 109–116.
[13] W. Lu, L. Dai, Carbon Nanotube Supercapacitors, in: J.M. Marulanda (Ed.), Carbon Nanotubes, InTech, 2010, pp. 563–589.
[14] K.H. An, W.S. Kim, Y.S. Park, J.M. Moon, D.J. Bae, S.C. Lim, Y.S. Lee, Y.H. Lee, Advanced Functional Materials 11 (2001) 387–392.
[15] G. Lota, K. Fic, E. Frackowiak, Energy & Environmental Science 4 (2011) 1592–1605.
[16] Y. Chen, X. Zhang, P. Yu, Y.W. Ma, Journal of Power Sources 195 (2010) 3031–3035.
[17] Y. Yamada, O. Kimizuka, O. Tanaike, K. Machida, S. Suematsu, K. Tamamitsu, S. Saeki, Y. Yamada, H. Hatori, Electrochemical and Solid State Letters 12 (2009) K14–K16.
[18] A. Izadi-Najafabadi, D.N. Futaba, S. Iijima, K. Hata, Journal of the American Chemical Society 132 (2010) 18017–18019.
[19] A. Izadi-Najafabadi, T. Yamada, D.N. Futaba, M. Yudasaka, H. Takagi, H. Hatori, S. Iijima, K. Hata, ACS Nano 5 (2011) 811–819.
[20] A. Izadi-Najafabadi, S. Yasuda, K. Kobashi, T. Yamada, D.N. Futaba, H. Hatori, M. Yumura, S. Iijima, K. Hata, Advanced Materials 22 (2010) E235–E241.
[21] D.N. Futaba, K. Hata, T. Yamada, T. Hiraoka, Y. Hayamizu, Y. Kakudate, O. Tanaike, H. Hatori, M. Yumura, S. Iijima, Nature Materials 5 (2006) 987–994.
[22] A.R. Boccaccini, J. Cho, J.A. Roether, B.J.C. Thomas, E.J. Minay, M.S.P. Shaffer, Carbon 44 (2006) 3149–3160.
[23] L. Besra, M. Liu, Progress in Materials Science 52 (2007) 1–61.
[24] J. Cho, K. Konopka, K. Rozniatowski, E. Garcia-Lecina, M.S.P. Shaffer, A.R. Boccaccini, Carbon 47 (2009) 58–67.
[25] I. Corni, M.P. Ryan, A.R. Boccaccini, Journal of the European Ceramic Society 28 (2008) 1353–1367.
[26] C.S. Du, D. Heldbrant, N. Pan, Materials Letters 57 (2002) 434–438.
[27] M.D. Lima, M.J. de Andrade, C.P. Bergmann, S. Roth, Journal of Materials Chemistry 18 (2008) 776–779.
[28] B.J.C. Thomas, A.R. Boccaccini, M.S.P. Shaffer, Journal of the American Ceramic Society 88 (2005) 980–982.
[29] B.J.C. Thomas, M.S.P. Shaffer, S. Freeman, M. Koopman, K.K. Chawla, A.R. Boccaccini, Electrophoretic Deposition of Carbon Nanotubes on Metallic Surfaces, in: A.R.V.O.C.R. Boccaccini (Ed.), Electrophoretic Deposition: Fundamentals and Applications II, 2006, pp. 141–146.
[30] Z.M. Markovic, D.B. Perusko, D.D. Tosic, N.Z. Romcevic, M.D. Dramicanin, Z.M. Nikolic, B.M.T. Markovic, Hemijska Industrija 65 (2011) 363–370.
[31] A.G. Osorio, I.C.L. Silveira, V.L. Bueno, C.P. Bergmann, Applied Surface Science 255 (2008) 2485–2489.
[32] B. Smith, K. Wepasnick, K.E. Schrote, A.H. Bertele, W.P. Ball, C. O'Melia, D.H. Fairbrother, Environmental Science & Technology 43 (2009) 819–825.
[33] B. Smith, K. Wepasnick, K.E. Schrote, H.-H. Cho, W.P. Ball, D.H. Fairbrother, Langmuir 25 (2009) 9767–9776.
[34] Y.-T. Shieh, J.-Y. Chen, Y.-K. Twu, W.-J. Chen, Polymer International (2011).
[35] L.L. Zeng, L. Zhang, A.R. Barron, Nano Letters 5 (2005) 2001–2004.
[36] P. Sattari, S. Ilhan, J.Z. Wen, S. Jayaram, in: Numerical Modeling of Electrical and Thermal Behaviors of Supercapacitors During Charging/Discharging, Waterloo (2012).
[37] M. Farbod, S.K. Tadavani, A. Kiasat, Colloids and Surfaces A – Physicochemical and Engineering Aspects 384 (2011) 685–690.
[38] S. Brunauer, P.H. Emmett, E. Teller, Journal of the American Chemical Society 60 (1938) 309–319.
[39] E.P. Barret, P.B. Joyner, P. Halenda, Journal of the American Chemical Society 73 (1951) 373–380.
[40] J.J. Moore, J.H. Kang, J.Z. Wen, Materials Chemistry and Physics 134 (2012) 68–73.
[41] J.J.E. Moore, J.H. Kang, S.H. Jayaram, J.Z. Wen, Journal of Applied Electrochemistry 42 (2012) 501–508.
[42] Y.S. Joung, C.R. Buie, Langmuir 27 (2011) 4156–4163.
[43] A.Y. Wu, P.M. Vilarinho, A.I. Kingon, Journal of American Ceramic Society 89 (2006) 575–581.
[44] L.-X. Li, F. Li, New Carbon Materials 26 (2011) 224–228.
[45] Y.T. Kim, Y. Ito, K. Tadai, T. Mitani, U.S. Kim, H.S. Kim, B.W. Cho, Applied Physics Letters 87 (2005).